Available online at www.sciencedirect.com

ScienceDirect

www.elsevier.com/locate/jes

JES JOURNAL OF ENVIRONMENTAL SCIENCES

www.jesc.ac.cn

Removing and recycling mercury from scrubbing solution produced in wet nonferrous metal smelting flue gas purification process

Shu Yang[2], *Ziliang Li*[1], *Kang Yan*[1,3], *Xi Zhang*[1], *Zhifeng Xu*[1,3], *Wanrong Liu*[4], *Zhilou Liu*[1,3,*], *Hui Liu*[2,*]

[1] *School of Metallurgy Engineering, JiangXi University of Science and Technology, Ganzhou 341000, China*
[2] *School of Metallurgy and Environment, Central South University, Changsha 410083, China*
[3] *Institute of Green Metallurgy and Process Intensification, Ganzhou 341000, China*
[4] *Solid Waste and Chemicals Management Center, Ministry of Environmental Protection, Beijing 100024, China*

ARTICLE INFO

Article history:
Received 2 August 2020
Revised 13 October 2020
Accepted 13 October 2020
Available online 30 October 2020

Keywords:
Mercury
Electrodeposition
Scrubbing solution
Pollution control

ABSTRACT

Wet purification technology for nonferrous metal smelting flue gas is important for mercury removal; however, this technology produces a large amounts of spent scrubbing solution that contain mercury. The mercury in these scrubbing solutions pose a great threat to the environment. Therefore, this research provides a novel strategy for removing and recycling mercury from the scrubbing solution, which is significant for decreasing mercury pollution while also allowing for the safe disposal of wastewater and a stable supply of mercury resources. Some critical parameters for the electrochemical reduction of mercury were studied in detail. Additionally, the electrodeposition dynamics and electroreduction mechanism for mercury were evaluated. Results suggested that over 92.4% of mercury could be removed from the scrubbing solution in the form of a Hg-Cu alloy under optimal conditions within 150 min and with a current efficiency of approximately 75%. Additionally, mercury electrodeposition was a quasi-reversible process, and the controlled step was the mass transport of the reactant. A pre-conversion step from $Hg(Tu)_4^{2+}$ to $Hg(Tu)_3^{2+}$ before mercury electroreduction was necessary. Then, the formed $Hg(Tu)_3^{2+}$ on the cathode surface gained electrons step by step. After electrodeposition, the mercury in the spent cathode could be recycled by thermal desorption. The results of the electrochemical reduction of mercury and subsequent recycling provides a practical and easy-to-adopt alternative for recycling mercury resources and decreasing mercury contamination.

Introduction

Mercury pollution has attracted the world's attention due to its global communication, high toxicity and potential for biomagnification. To date, over 150 countries have agreed to the Minamata Convention on Mercury, which is designed to reduce global mercury emissions (Agarwalla et al., 2020). The nonferrous metal smelting industry is one of the major anthropogenic sources of mercury release (Huang et al., 2017; Wu et al., 2018; Liu et al., 2020). Large amounts of mercury-containing contaminants are produced during smelting pro-

* Corresponding author.
E-mails: lzl8786489@163.com (Z. Liu), huiliucsu@163.com (H. Liu).

https://doi.org/10.1016/j.jes.2020.10.013
1001-0742/

cesses each year, and these contaminants cause great harm to the environment (An et al., 2019; Yan et al., 2019; Liu et al., 2017, 2019, 2020). Furthermore, the Minamata Convention on Mercury requires the elimination of primary mercury mining. However, mercury still has a variety of applications in many industries, such as chlor-alkali and acetaldehyde production. Predictably, mercury-containing secondary resources will become the main source of mercury and ensure mercury supply in the future (Cunha et al., 2016; Seung-KiBack et al., 2019). Therefore, from the perspective of environmental conservation and mercury recycling, it is necessary to reduce mercury pollution and recover mercury resources from the nonferrous metal smelting industry.

Nearly all mercury in metallic minerals is transferred to the flue gas in the process of roasting or smelting (Huang et al., 2017; Hu et al., 2020). Many techniques, including adsorption, catalytic oxidation and wet purification, have been reported for mercury removal in flue gas (Zhang et al., 2020; Yang et al., 2019; Zou et al., 2017; Ma et al., 2019; Yang et al., 2019; Yang et al., 2019; Liu et al., 2020; Zhang et al., 2020; Zhang et al., 2020). Among these, wet purification is recognized as a promising technology and has been widely used because it can synergistically remove multiple pollutants with a low cost and high efficiency (Ma et al., 2014; Liu et al., 2017; Liu et al., 2017). To promote mercury oxidation and removal from smelting flue gas containing a high concentration of SO_2 (Liu et al., 2017, 2019), some additives, such as thiourea (Tu), are added to acidic scrubbing solutions due to its strong affinity with mercury (Liu et al., 2017). In addition, many metal impurities, such as ferric ions and cupric ions, also simultaneously enter the acidic thiourea scrubbing solution during wet purification, resulting in the formation of acidic wastewater with high concentrations of mercury and complex components. Currently, the removal and recovery of mercury from a complex scrubbing solution is challenging.

Most recently, various sorbents, such as metal oxides, metal sulfides and active carbon, have been increasingly studied for mercury removal from wastewater (Li et al., 2018; Tao et al., 2016; Liu et al., 2019; Huang et al., 2017; Li et al., 2018; Chen et al., 2019). However, they are not suitable for mercury removal from scrubbing solutions for smelting flue gas. Generally, the scrubbing solution is highly acidic and contains a high concentration of thiourea. The mercury species in a scrubbing solution is a mercury coordination compound $HgTu_4^{2+}$ (Liu et al., 2017) . In this case, the removal efficiency of mercury using traditional sorbents will be substantially hindered. Electrodeposition is a selective and efficient technique for removing and extracting metal or metallic compounds (Zhang et al., 2020; Robotin et al., 2013; Wang et al., 2018; Hu et al., 2019; Xu et al., 2020; Yang et al., 2020; Zhang et al., 2020). Various metal ions can be selectively reduced to the corresponding metal or metallic oxide by controlling redox reaction potentials. Zhang et al. (2020) used an electrodeposition method to selectively remove zinc and lead from a simulated smelting wastewater. Jin et al. (2018) adopted electrochemical extraction to recycle dilute copper and tellurium from acidic chloride solutions. Consequently, electrodeposition should be a scientifically feasible technique for the efficient removal and recycling of mercury. Unfortunately, few correlative studies have reported the mercury removal and recycling performance from a thiourea scrubbing solution utilized in a wet purification process for nonferrous metal smelting flue gas.

This study aims to develop an efficient process for the removal and extraction of mercury from a thiourea scrubbing solution. Some parameters in the electrodeposition process, including the applied potential, current density, electrolytic time and electrolyte composition, were investigated. Additionally, the mercury removal efficiency was systematically evaluated to elucidate the optimized conditions for this technology. Additionally, the electroreduction mechanism of mercury was proposed, leading to an alternative method for mercury-containing wastewater remediation and the sustainable utilization of mercury resources.

1. Experimental section

1.1. *Materials and electrolytic solution preparation*

All reagents, such as thiourea, ferric sulfate, copper sulfate and sodium sulfite, were analytically pure (Sinopharm Group Co.). Some standard graphite and copper sheets (20 mm wide, 30 mm long and 1.5 mm thick) were prepared. The obtained graphite and copper sheets, which were used as electrodes, were successively polished using 400- and 800-grade silicon carbide paper to guarantee smooth surfaces. The electrolytic solution was prepared by dissolving the required reagents in ultrapure water (18 MΩ•cm). The components in the typical electrolytic solution are shown in Appendix A Table S1.

1.2. *Electrodeposition studies*

A schematic diagram of the electrodeposition apparatus is shown in Appendix A Fig. S1. All electrodeposition tests, including linear sweep voltammetry, constant voltage electrolysis and cyclic voltammetry, were conducted with a CHI660 workstation. A sealed 100 mL three-electrode cell was applied with the prepared copper sheet as the working electrode, graphite as the counter electrode and silver chloride as the reference electrode (the purities of the copper and graphite sheets were over 99.99%). The inter-electrode distance between the working electrode and counter electrode was 12 mm. Before every test, the copper sheet electrode was immersed in 0.5 mol/L hydrochloric acid for over 2 hr to fully dissolve surface oxides. Subsequently, the copper sheet was cleaned with deionized water under ultrasonic conditions. The prepared electrolytic solution was added to the electrolytic cell, and the electrode couple (an active area of 4 cm^2) was connected to the constant-voltage power supply of the electrochemical workstation. Then, the electrolytic cell was placed in a water bath to control the temperature of the electrolytic solution. At this point, electrolysis with a constant current was applied to remove mercury. A good air-tight seal should be maintained throughout the experiment to avoid the volatilization of mercury. During the electrolytic process, a small amount of electrolytic solution was taken at regular intervals to analyse the mercury content. The mercury removal efficiency (R_{Hg}) can be described by the following Eq. (1).

$$R_{Hg} = \frac{C_0 - C_t}{C_0} \times 100\% \quad (1)$$

where C_0 (mg/L) is the initial concentration of mercury in the electrolytic solution and C_t (mg/L) is the measured concentration of mercury in the sample.

1.3. *Metallic mercury recycling*

As shown in Appendix A Fig. S2, thermal desorption and condensation technology were employed to recover metallic mercury. First, the spent cathode was placed in the middle of a tube furnace. Then, high purity nitrogen was used as the carrier gas to take gaseous elemental mercury. The tube furnace was heated from room temperature to 350°C at a heating rate of 5 °C/min with a nitrogen volume flow rate of 0.2 L/min. The holding time at 350°C was 120 min to guarantee the complete desorption of mercury. The gaseous elemental mercury was condensed into liquid metal mercury in a U-type tube which was placed in a chiller plant. Finally, the liquid metal mercury was collected from the bottom of U-type. The obtained off-gas containing mercury after condensation was adsorbed by a 2 mol/L potassium permanganate solution and activated carbon, thereby ensuring the safe disposal of mercury-containing gas.

1.4. *Analysis and characterization*

The mercury concentration in the electrolytic solution was determined by cold-vapor atomic absorption spectrometry (CVAAS; S-H-22, Themo Jarrell Ash Corporation, USA). All samples were measured three times with a relative standard deviation of less than 15%, and the arithmetic mean values were taken as the final data. Linear sweep voltammetry and cyclic voltammetry were carried out in N_2-purged electrolytic solution at room temperature. Scanning electron microscopy (SEM, Nova Nano230, USA) was used to identify the surface morphology of the deposit. The metallic composition on the cathode surface was analysed by energy dispersive X-ray spectroscopy (EDS, Oxford X-act, UK).

2. Results and discussion

2.1. *Determination of the reduction potential for mercury removal*

Linear sweep voltammetry investigations were performed to determine the electrochemical reduction potential of mercury on the copper sheet electrode, and the corresponding results are illustrated in Fig. 1. As shown in Fig. 1a, two obvious reduction peaks appeared at approximately -0.53 and -0.72 V in the mixed solution containing H_2SO_4, Tu and Hg^{2+}, respectively. Some hydrogen gas bubbles appeared when the potential was lower than -0.72 V, indicating the peak at -0.72 V represented the hydrogen evolution reaction. In addition, no cathodic peak at -0.53 V was found in the contrast experiment when no Hg^{2+} was added to the electrolyte. This result implied that the peak at -0.53 V was the reduction of mercury. Appendix A Fig. S3 shows that the reduction potential of Hg^{2+} in the absence of Tu was approximately -0.34 V. The mercury species in the electrolyte should be stable $Hg(Tu)_x^{2+}$ complexes in the presence of Tu due to a strong affinity between Hg^{2+} and Tu. The formation of $Hg(Tu)_x^{2+}$ resulted in a negative shift of the cathodic peak for Hg^{2+} reduction. According to the stability constants of the different $Hg(Tu)_x^{2+}$ complexes, the final mercury species product was $Hg(Tu)_4^{2+}$ when in excess Tu. Hence, the electrodeposition process of mercury can be expressed by Eq. (2).

$$Hg(Tu)_4^{2+} + 2e = Hg + 4Tu \quad (2)$$

Some reducible impurities in the electrolytic solution may affect the mercury reduction potential. Fig. 1b shows the effect of H_2SO_3 on mercury reduction. When the potential was lower than -0.6 V, the current density clearly increased in the presence of H_2SO_3. The same phenomenon also occurred in the curve of the mixed solution containing H_2SO_4, Tu, H_2SO_3 and Hg^{2+}. Previous studies (Quijada et al., 2000; Yang et al., 2017) reported that H_2SO_3 could be reduced to low valence compounds, such as $S_2O_3^{2-}$ and $S_4O_6^{2-}$, when the potential was lower than -0.6 V, indicating that the reduction of H_2SO_3 could occur at low potential. The reduction product of H_2SO_3, such as $S_2O_3^{2-}$, is unstable in an acidic solution and easily decomposes into elemental sulfur, which can deposit on the electrode and affect the electrolytic process (Han et al., 2017). Clearly, the cathode potential should not exceed -0.6 V to avoid the effect of H_2SO_3 reduction.

It is easy to reduce Fe^{3+} to Fe^{2+} at a negative potential. However, the cathode current density shows no significant increase in the curve of the mixed solution containing H_2SO_4, Tu and Fe^{3+} in Fig. 1c. This result was probably because of the formation of stable $Fe(Tu)_x^{3+}$ in the solution with a high concentration of Tu, thus reducing the reduction activities of Fe^{3+} on the cathode. A weak reduction peak of Fe^{3+} appeared at -0.62 V in the mixed solution of H_2SO_4, Tu, Fe^{3+} and Hg^{2+}. This result also implied that Hg^{2+} would be preferentially reduced over Fe^{3+} in an acidic Tu solution. Therefore, the presence of Fe^{3+} did not affect mercury electrodeposition if the potential is controlled. As shown in Fig. 1d, three peaks appeared in the curve of the mixed solution containing H_2SO_4, Tu, Cu^{2+} and Hg^{2+}. The peaks at approximately -0.28 and -0.69 V were related to the $Cu(Tu)_x^{2+}$ reduction to $Cu(Tu)_x^{+}$ and the $Cu(Tu)_x^{+}$ reduction to Cu, respectively. The peak at -0.48 V was due to the combination reaction of Hg^{2+} and Cu^{2+}, suggesting the possible simultaneous reduction of Hg^{2+} and Cu^{2+}. The Cu^{2+} in the electrolyte could lead to the obtained potential positively shifting to approximately 0.5 V from -0.53 to -0.48 V, which would be particularly beneficial for the electrochemical deposition of mercury. Although Cu^{2+} was preferentially reduced to $Cu(Tu)_x^{+}$ over Hg^{2+} in an acidic Tu solution, the preferential deposition of mercury could still be obtained because the reduction potential of mercury from $Hg(Tu)_4^{2+}$ to Hg was higher than that of copper from $Cu(Tu)_x^{+}$ to Cu. Namely, copper would not deposit on the cathode when the cathode potential was between -0.55 and -0.4 V. In summary, mercury could be separated and recycled from an acidic Tu solution by electrodeposition, and the optimum reduction potential was approximately -0.55 and -0.4 V.

2.2. *Electrodeposition of mercury*

Constant current electrolysis is a common method to obtain metals by reduction and deposition in industry. In this study, the effect of current density on mercury removal efficiency and current efficiency over time was evaluated with

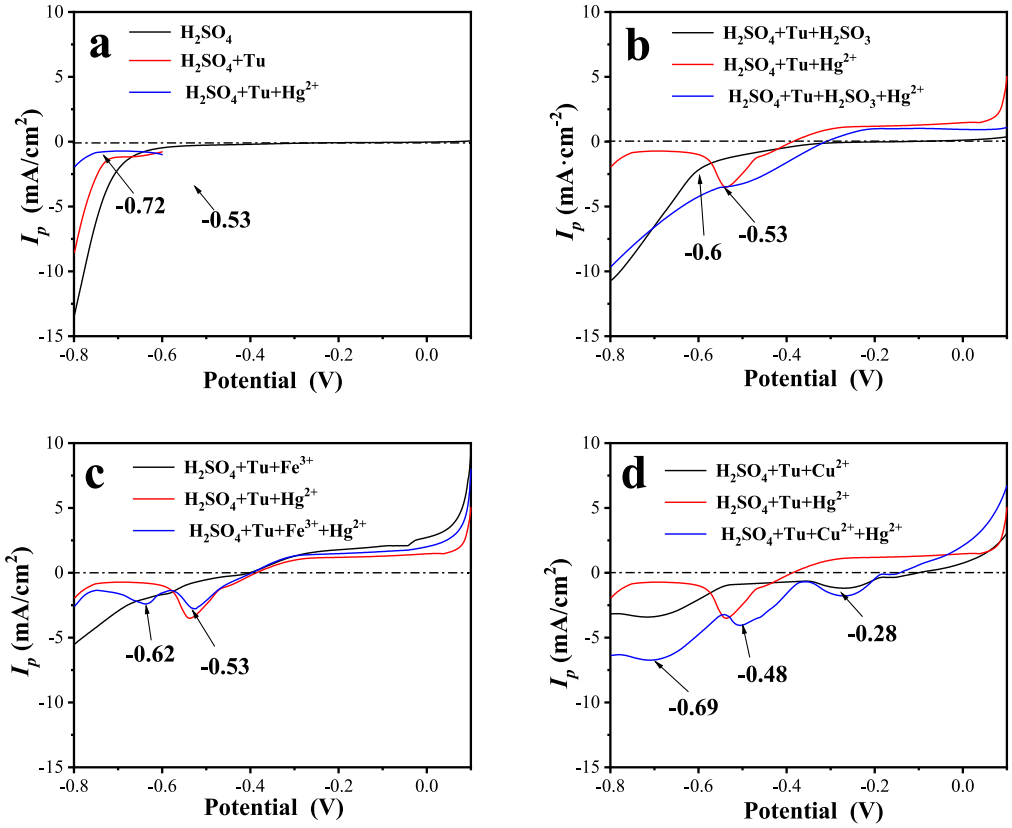

Fig. 1 – Linear sweep voltammetry for mercury reduction from an (a) acidic Tu solution, (b) acidic Tu solution containing H_2SO_3, (c) acidic Tu solution containing Fe^{3+} and acidic Tu solution containing Cu^{2+}. Experimental conditions: scan rate was 5 mV/sec; solution pH was 0.5; Tu, H_2SO_3, Fe^{3+} and Cu^{2+} concentrations were 150, 8, 20 and 20 mmol/L, respectively, if present in the test.

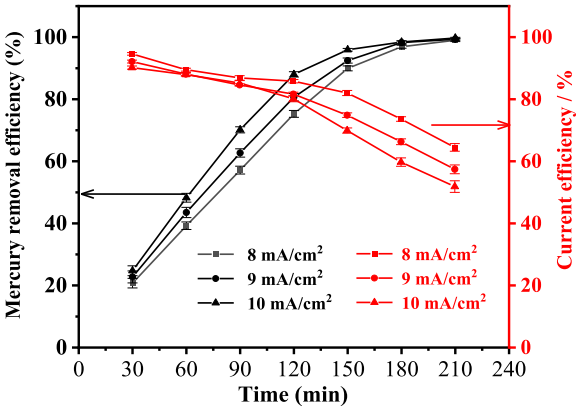

Fig. 2 – Effect of the current density on the mercury removal efficiency and current efficiency in the electrodeposition process. Experimental conditions: temperature = 25°C; stirring rate = 300 r/min; pH = 0.5; Tu, SO_3^{2-}, Fe^{3+} and Cu^{2+} concentrations were 150, 8, 20 and 20 mmol/L, respectively.

a cathode voltage between -0.55 and -0.4 V to ensure the selective removal of mercury. The results in Fig. 2 indicate that the mercury removal efficiency increased linearly over time within 120 min. The corresponding current efficiency remained at approximately 80%. The increase in current density from 8 to 10 mA/cm^2 benefitted mercury removal. After electrolysis for 210 min, the mercury removal efficiency could reach over 95%, proving the feasibility of electrodeposition for mercury removal. When the electrolysis time was over 150 min, the current efficiency declined sharply. At the later stage of electrolytic deposition, the mercury concentration in the electrolyte decreased, and the corresponding cathode voltage shifted negatively, resulting in the appearance of side reactions, such as the reduction of $Fe(Tu)_x^{3+}$ and copper deposits.

Fig. 3 shows the mercury removal efficiency and current efficiency as a function of the Tu, H_2SO_3, Fe^{3+} and Cu^{2+} concentrations in the electrolyte. As shown in Fig. 3a, the mercury removal efficiency and current efficiency decreased with increasing Tu concentrations. For example, the mercury removal efficiency and current efficiency after 120 min of electrodeposition were 88.2% and 85.4% in a 50 mmol/L Tu solution, respectively. However, they decreased to 72.4% and 73.5% as the Tu concentration increased to 150 mmol/L, respectively. There were two possible reasons for the decrease in mercury removal efficiency and current efficiency. One possible reason was that the stability of $Hg(Tu)_4^{2+}$ increased with Tu concen-

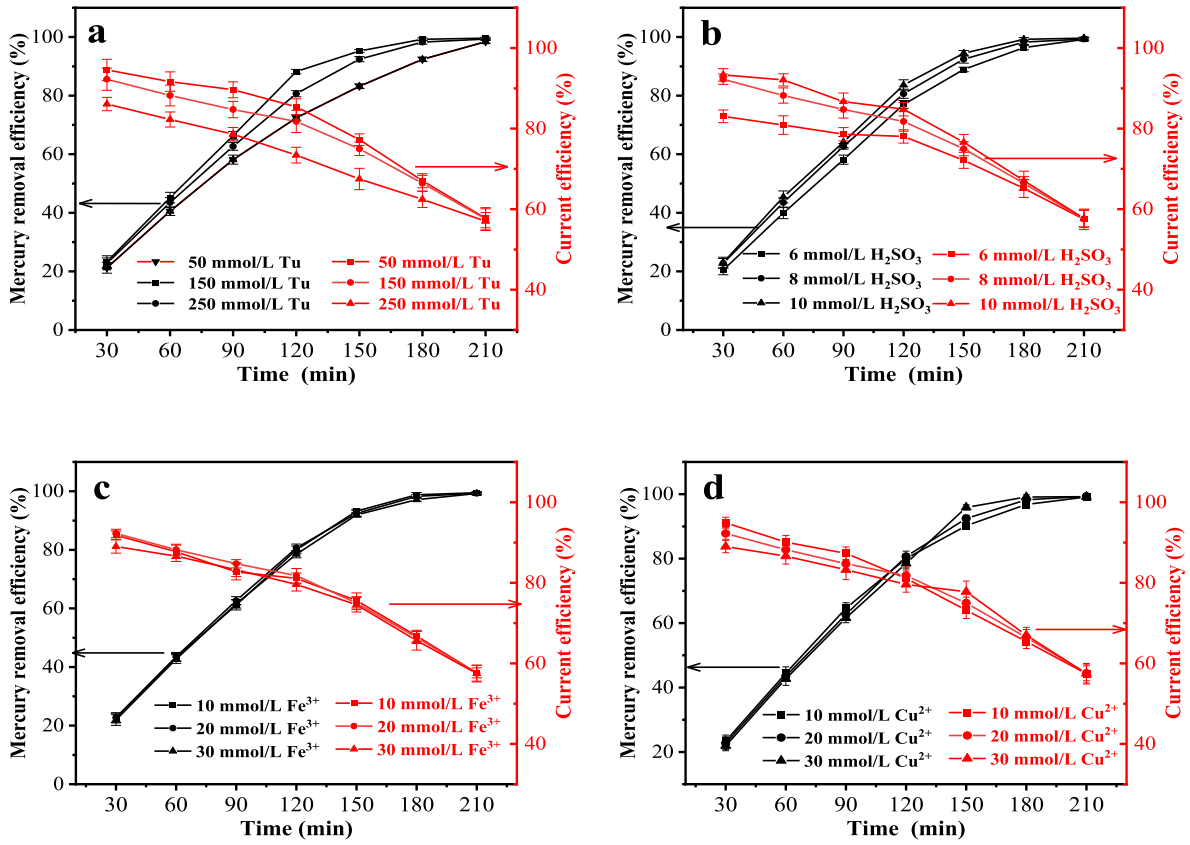

Fig. 3 – Effect of the Tu (a), H_2SO_3 (b), Fe^{3+} (c) and Cu^{2+} (d) concentrations on the mercury removal efficiency and current efficiency in the electrodeposition process. Experimental conditions: temperature = 25°C; current density = 9 mA/cm^2; stirring rate = 300 r/min; pH = 0.5; Tu, SO_3^{2-}, Fe^{3+} and Cu^{2+} concentrations were 150, 8, 20 and 20 mmol/L, respectively, except for when it was a variable.

tration, which opposed the reduction of mercury on the cathode. During the electrolysis process, a portion of Tu would inevitably oxidize on the anode to form intermediate oxidation products, such as formamidine disulfide. Previous literature (Han et al., 2017) reported that the intermediate oxidation product of Tu could be reduced to Tu. Therefore, another reason might be the side reaction of Tu oxidation and reduction, which would result in the decreases in mercury removal efficiency and current efficiency.

As presented in Fig. 3b, the presence of H_2SO_3 benefited mercury removal. With the increase in H_2SO_3 from 6 to 10 mmol/L, the mercury removal efficiency and current efficiency slightly increased. According to a previous report (Liu et al., 2017), the existence of H_2SO_3 could inhibit the oxidation of Tu in solution. Thus, the decrease in the intermediate oxidation product of Tu might lead to an enhanced mercury removal performance. The electrochemical performance did not change with the Fe^{3+} concentration (see Fig. 3c), indicating that the presence of Fe^{3+} had little effect on mercury removal. In contrast, Cu^{2+} had a different role on mercury removal efficiency at different electrolysis time (see Appendix A Fig. S5). At the initial stage of electrodeposition, the increase in Cu^{2+} concentration hindered mercury removal because of the interference of Cu^{2+} reduction. However, the presence of Cu^{2+} could accelerate the mercury removal efficiency and current efficiency at the late stage of electrodeposition. Appendix A Fig. S4 shows that the cathode potential increases to over -0.6 V at the late stage of electrodeposition, in which the co-deposition of metallic copper and mercury may appear. The co-deposition of mercury and copper on the cathode decreased the mercury electrodeposition potential, which benefitted mercury removal and resulted in an increase in mercury removal performance at high Cu^{2+} concentrations.

The reaction temperature and pH are important parameters for the electrolytic deposition of mercury. The effects of reaction temperature and pH on mercury removal performance are presented in Appendix A Figs. S6 and Fig. S7, respectively. The results suggested that the mercury removal performances had little change in the reaction temperature range of 10 to 40°C. Further increasing reaction temperature from 40 to 70°C, the mercury removal efficiency increased, while the current efficiency decreased. The copper reduction and deposition rate increased with temperature, resulting in the formation of Hg-Cu alloy and promoting the mercury electrodeposition. However, the increase of mercury removal performance is limited, only from 92.5% to 94.3%. Therefore, the rise of temperature will not significantly improve the mercury removal performance. Appendix A Fig. S7 indicated that the

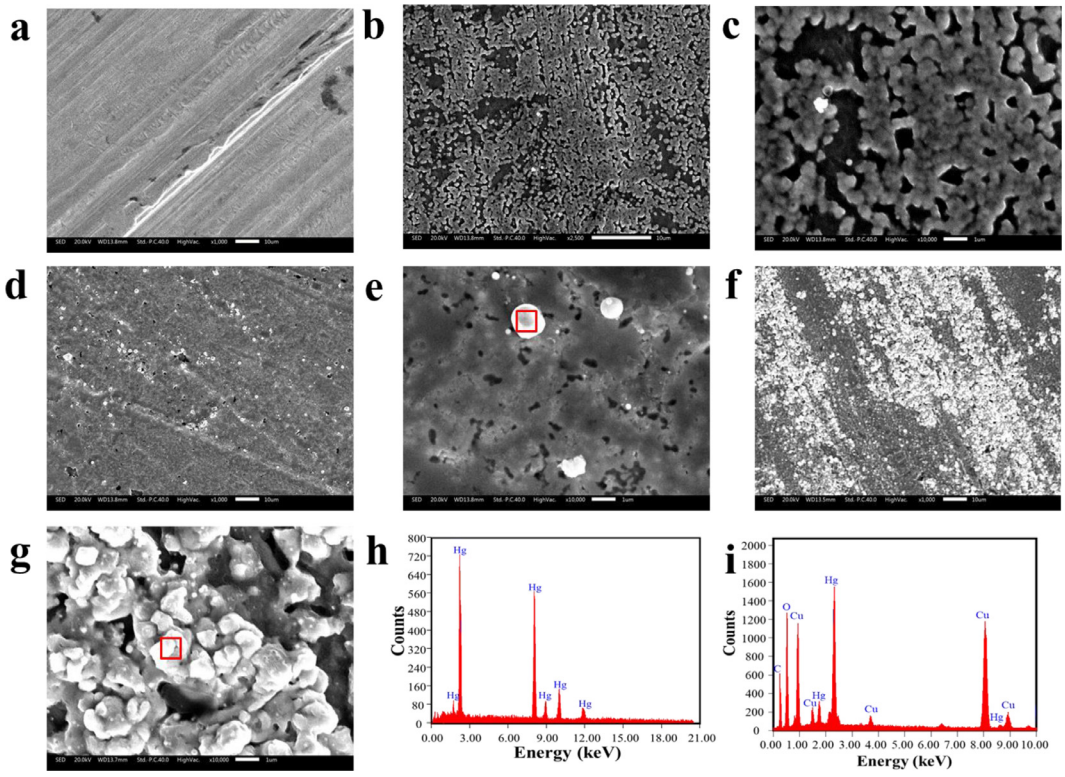

Fig. 4 – SEM images of the mercury deposition at the copper electrode with electrolysis time of 0 (a), 20 (b and c), 40 (d and e) and 240 min (f and g). EDS results (h and i) of the electrodeposited product in the marked square.

mercury removal performance was almost invariant in the pH range of 0 to 1.5, while decreased with further increasing pH value to 3. The formation of $Fe(OH)_3$ colloid and the occurrence of side reactions of Tu oxidation and reduction could be the reason for the reduction of mercury removal efficiency. Additionally, the pH of actual scrubbing solution is usually below 1. Therefore, the optimal pH value is below 0.5 from the views of practical applications and removal performance.

2.3. *Product characterization*

To illustrate the evolution behaviour for mercury electrodeposition at different electrolytic time, the morphology of the mercury deposit is depicted in Fig. 4. Compared with the morphology of the cathode before electrodeposition in Fig. 4a, the nucleation and growth of mercury deposits in Fig. 4b and 4c continuously increased, gradually covering the cathode. Upon further extension of the electrolysis time to 40 min, some spheres with a diameter of approximately 100 nm appeared in Fig. 4d and 4e. The corresponding EDS mapping results in Fig. 4h confirm that these spheres are mainly composed of hydrargyrum. After 210 min of electrolysis, many aggregate particles appeared on the cathode surface. The EDS result suggested the existence of Cu. Additionally, the concentration of Cu^{2+} in the electrolyte was detected to avoid the interference of copper cathode. The results showed that the copper content in the electrolyte decreased by approximately 12.3% after electrochemical reduction, which confirmed the electrodeposition of copper. These results suggested that the main product of electrolysis at the late stage was a Hg-Cu alloy.

2.4. *Electrodeposition dynamics*

The kinetic analyses for mercury reduction from an acidic scrubbing solution were studied using cyclic voltammetry to further characterize the electrodeposition behaviour. Fig. 5a presents the current density as a function of potential at different scan rates. The potential of the reduction peak shifted in the negative direction, and the corresponding peak current increased with an increasing scan rate, which was in accordance with a quasi-reversible reaction. Additionally, good linearity between the peak currents (I_p) and square root of the scan rate (v) was obtained, as shown in Fig. 5b, implying that the dynamic control step was diffusion control. The peak currents I_p can be expressed by the following Eq. (3).

$$I_p = 0.4463n^{3/2}AF^{3/2}RT^{-1/2}D^{1/2}C_0V^{1/2} \quad (3)$$

where I_p (A) is the peak current, n is the number of electrons transferred for mercury reduction, A (cm^2) is the working area of the cathode, D (cm^2/sec) is the diffusion coefficient, C_0 (mol/cm^3) is the concentration of the reactant, and V (V/sec) is the scan rate. The diffusion coefficient D for mercury reduction was calculated as 3.3×10^{-4} cm^2/sec, which was not high and would require enhancement to accelerate the mass transfer process.

The effect of the stirring rate on the cathode peak current density was investigated. As shown in Fig. 6a, the peak cur-

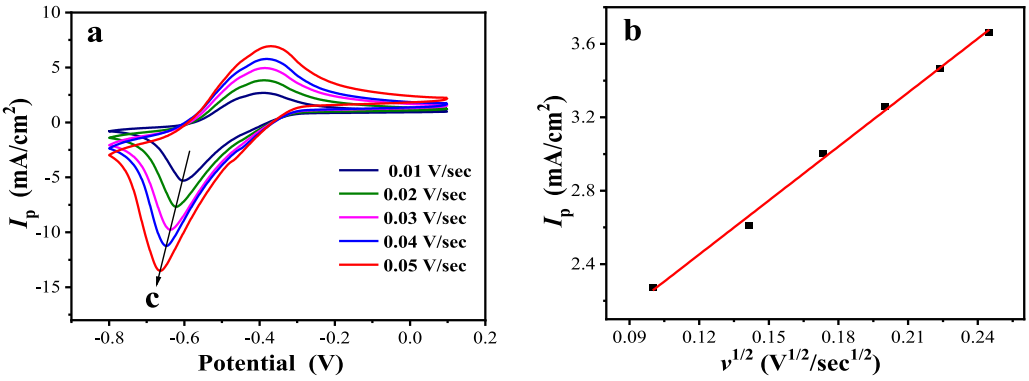

Fig. 5 – (a) Cyclic voltammetry curve of the Tu solution for mercury reduction from an acidic Tu solution at different scan rates, and (b) the variation in the mercury reduction peak current density as a function of the square root of the scan rate from 0.01 to 0.05 V/sec.

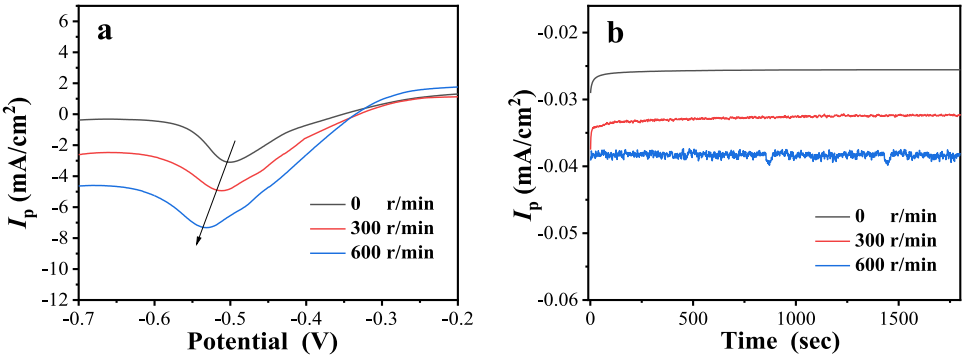

Fig. 6 – (a) Linear sweep voltammetry curves (scan rate of 10 mV/sec) and (b) chronoamperometry curves for mercury reduction at different stirring rates.

rent density increased with increasing stirring rate, suggesting the beneficial effects of increasing the stirring rate for mercury electrodeposition. This finding also confirmed that the dynamic control step for mercury electrodeposition was the mass transfer of the reactant. The obtained current density in Fig. 6b increased from -0.025 mA/cm^2 without stirring to -0.038 mA/cm^2 at a stirring rate of 600 r/min. Therefore, enhancing the mass transfer process by increasing the stirring rate benefitted the performance of mercury electrodeposition.

2.5. *Mechanism of mercury reduction*

From Section 2.1, the mercury species in the electrolyte was high coordination $Hg(Tu)_4^{2+}$. During the electroreduction of metal complexes, there are two possible reaction paths. In this case, one was the direct reduction of $Hg(Tu)_4^{2+}$ on the cathode. The other was a pre-conversion step from high coordination $Hg(Tu)_4^{2+}$ to low coordination $Hg(Tu)_x^{2+}$ (x of less than 4) before the electroreduction of $Hg(Tu)_4^{2+}$ first occurred. Subsequently, the formed $Hg(Tu)_x^{2+}$ would be reduced to metallic mercury. The constant current step technique was used to verify the reduction step of $Hg(Tu)_4^{2+}$ on the copper cathode. According to the Sand equation Powell et al., 2007), $i\tau^{1/2}$ met Eqs. (4) and ((5) with and without the pre-conversion step, respectively. The equations are described as follows:

$$i\tau^{1/2} = \frac{nF\pi^{1/2}D^{1/2}C_0}{2} - \frac{\pi^{1/2}C_{Tu}{}^{4-x}i}{2K(k_1+k_{-1})^{1/2}} \quad (4)$$

$$i\tau^{1/2} = \frac{nF\pi^{1/2}D^{1/2}C_0}{2} \quad (5)$$

where i (mA) is the current, τ (sec) is the transient time, n is the number of transferred electrons, F is the Faraday constant, D (cm^2/sec) is the diffusion coefficient, C_0 (mol/L) is the initial concentration of the reactant, k_1 and k_2 are the reaction rate constants of the forward and reverse reactions of the pre-conversion step, respectively, K is the ratio of k_1 and k_2, and C_{Tu} (mol/L) is the concentration of thiourea. Fig. 7a shows the potential changes at a constant current step of 1 mA. The corresponding transient time was 13.59 sec. The transient time at different step currents are shown in Appendix A Table S3. The results in Fig. 7b indicate a linear interrelationship between $i\tau^{1/2}$ and i, illustrating the presence of a pre-conversion step from $Hg(Tu)_4^{2+}$ to $Hg(Tu)_x^{2+}$ before the electroreduction of $Hg(Tu)_x^{2+}$. Therefore, Eq. (5) was suitable for describing the mercury reduction behaviour. To confirm the product after the

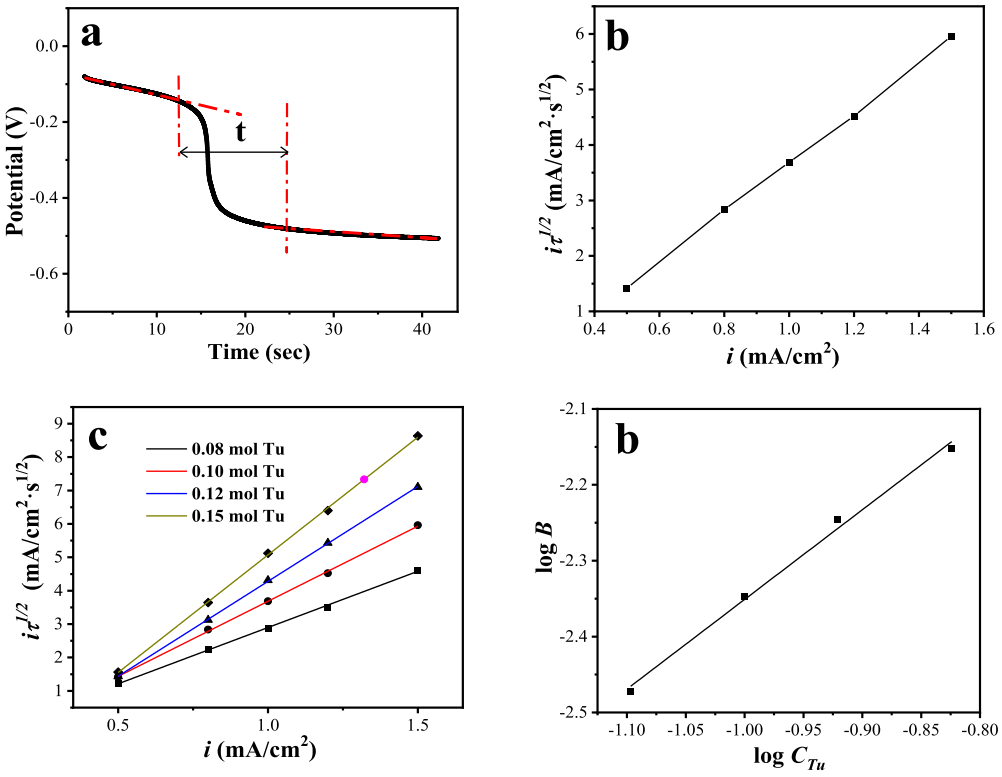

Fig. 7 – (a) Potential-time curve at a constant current step of 1 mA; (b) relationship between $i\tau^{1/2}$ and i at different currents; (c) relationship between $i\tau^{1/2}$ and i with different Tu concentrations; (d) relationship between the logarithmic slope and logarithmic Tu concentration.

pre-conversion step, the slope in Fig. 7c was converted by the following Eq. (6):

$$\log B = \log \frac{\pi^{1/2}}{2K(k_1 + k_{-1})^{1/2}} - (4 - x)\log C_{Tu} \quad (6)$$

where B represents the corresponding slope. Clearly, log$B$ was directly proportional to the log of Tu concentration. As shown in Fig. 7d, log$B$ and logC_{Tu} had a linear relationship, and the corresponding slope (4-x) was 1.16. This result suggested that the product of the pre-conversion step on the surface of the cathode should be $Hg(Tu)_3^{2+}$.

The electron transfer for mercury reduction from the electrolyte was studied. As presented in Appendix A Fig. S8, only one reduction peak appeared at approximately -0.57 V and a scan rate of 10 mV/sec. The peak evolved into two weak peaks when the scan rate dropped to 2 mV/sec. The appearance of two peaks in the area of mercury reduction confirmed that mercury reduction consisted of two consecutive one-electron transfer processes. The peak at approximately -0.55 V should be attributed to the first step of mercury reduction from $Hg(Tu)_3^{2+}$ to $Hg(Tu)_3^{+}$, and the peak at -0.59 V was ascribed to the second step of mercury reduction from $Hg(Tu)_3^{+}$ to Hg.

Based on the above discussions, a pre-conversion step on the surface of the cathode from $Hg(Tu)_4^{2+}$ to $Hg(Tu)_3^{2+}$ was needed before mercury electroreduction from the Tu solution. Subsequently, the formed $Hg(Tu)_3^{2+}$ gained electrons step by step, thereby forming elemental mercury as the final product.

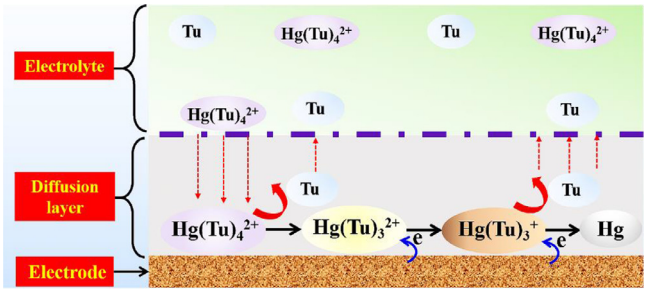

Fig. 8 – Schematic diagram of the electrolytic process at the cathode for the electrochemical reduction of mercury.

The schematic diagram showing the diffusion and reaction path on the cathode surface is presented in Fig. 8, helping facilitate a deep understanding of mercury electroreduction behaviour.

2.6. *Significance of metal mercury collection and practical application*

After mercury electrodeposition, thermal desorption technology was used to recycle metal mercury from the spent cathode. The result in Appendix A Fig. S9 shows that almost all of the mercury in the Hg-Cu alloy on the surface of the cathode can decompose to gaseous elemental mercury through

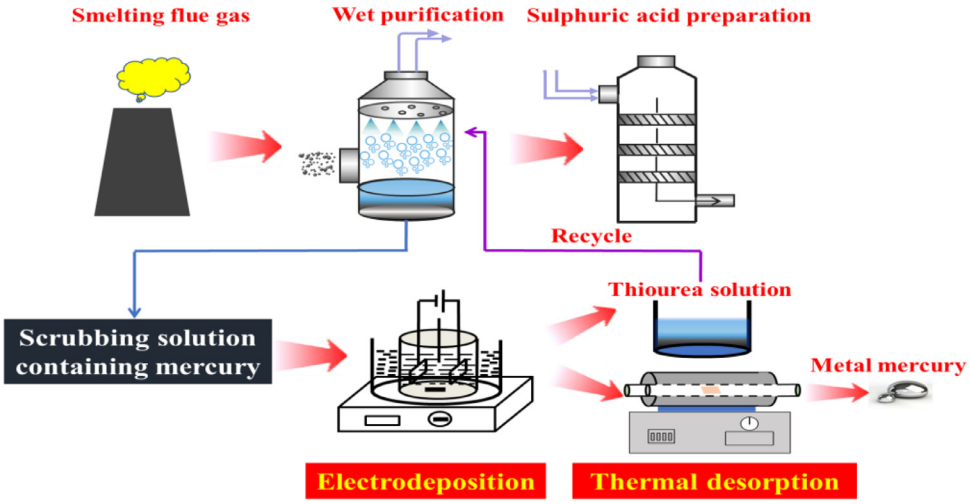

Fig. 9 – Practical application illustrating the electrolytic technology for recycling mercury and the scrubbing solution.

thermal desorption. Subsequently, the obtained gaseous elemental mercury was condensed into liquid metal mercury. Fig. 9 presents the practical application of electrolytic technology for mercury recycling and scrubbing solution recycling. The separation and recovery of mercury from the scrubbing solution could realize mercury resource utilization and avoid mercury contamination from nonferrous metal smelting. Additionally, the remaining thiourea solution after electrolysis could return to the flue gas purification system, which decreased the cost of mercury removal. Overall, electrodeposition technology has broad prospects in mercury resource utilization and provides a sustainable perspective for mercury removal from flue gas and mercury pollution control from wastewater.

3. Conclusions

In this study, a sustainable technology for mercury removal and recycling using electrochemical extraction from a scrubbing solution was proposed. Different parameters for mercury electrodeposition and kinetics were evaluated. The results show that the mercury in the scrubbing solution could be selectively electrodeposited by controlling the cathode potential. Over 92.4% of mercury could be recycled in the form of an amalgam under optimal conditions within 150 min and with a current efficiency of approximately 75%. The mercury electroreduction process was a quasi-reversible process with mass transport-controlled kinetics. The mechanistic study indicated a pre-conversion step from $Hg(Tu)_4^{2+}$ to $Hg(Tu)_3^{2+}$ before mercury electroreduction. The formed $Hg(Tu)_3^{2+}$ on the cathode surface gained electrons step by step, before finally being reduced to mercury. The electrodeposition method might provide a potential alternative technique for achieving mercury recovery and reducing mercury pollution, which would be conducive to the green and sustainable development of the nonferrous metal smelting industry. Further study is needed to operate the electrodeposition process in a turbulent reactor to enhance mass transport and improve the current efficiency, thereby benefiting industrial applications.

Acknowledgments

This work was supported by the Natural Science Foundation of China (No. 51804139), the China Postdoctoral Science Foundation (No. 2019M652275) and the Program of Qingjiang Excellent Young Talents of Jiangxi University of Science and Technology (No. 2019003).

Appendix A Supplementary data

Supplementary material associated with this article can be found, in the online version, at doi:10.1016/j.jes.2020.10.013.

REFERENCES

Agarwalla, H., Senapati, R.N., Das, T.B., 2020. Mercury emissions and partitioning from indian coal-fired power plants. J. Environ. Sci. 100, 28–33.
An, M., Ma, J., Guo, Q., 2019. Transformation and migration of mercury during chemical-looping gasification of coal. Ind. Eng. Chem. Res. 58 (44), 20481–20490.
Back, S.K., Lee, E.S., Seo, Y.C., Jang, H.N., 2019. The effect of naoh for the recovery of elemental mercury from simulated mixture wastes and waste sludge from an industrial process using a thermal desorption process. J. Hazard. Mater. 384, 121291.
Chen, L., Xu, H., Xie, J., Liu, X., Yuan, Y., Liu, P., et al., 2019. $[SnS_4]^{4-}$ clusters modified MgAl-LDH composites for mercury ions removal from acid wastewater. Environ. Pollut. 247, 146–154.
Cunha, R.C.D., Patrício, P.R., RodriguezVargas, S.J., Silva, L.H.M., Silva, M.C.H., 2016. Green recovery of mercury from domestic and industrial waste. J. Hazard. Mater. 304, 417–424.
Han, C., Wang, W., Xie, F., Zhang, T.A., 2017. Mechanism and kinetics of mercuric sulfide leaching with cuprous-thiosulfate solutions. Sep. Purif. Technol. 177, 223–232.

Hu, J., Sun, Q., Zhang, J.H., 2020. Critical temperature for rapid release of mercury from coal after high temperature: a review. J. Clean. Prod. 267, 122166.
Hu, M., Sun, Z., Hu, J., Lei, H., Jin, W., 2019. Simultaneous phenol detoxification and dilute metal recovery in cyclone electrochemical reactor. Ind. Eng. Chem. Res. 58 (28), 12642–12649.
Huang, N., Zhai, L., Xu, H., Jiang, D., 2017. Stable covalent organic frameworks for exceptional mercury removal from aqueous solutions. J. Am. Chem. Soc. 139 (6), 2428–2434.
Huang, Y., Deng, M., Li, T., Japenga, J., Chen, Q., Yang, X., et al., 2017. Anthropogenic mercury emissions from 1980 to 2012 in china. Environ. Pollut. 226, 230–239.
Jin, W., Hu, M., Hu, J., 2018. Selective and efficient electrochemical recovery of dilute copper and tellurium from acidic chloride solutions. ACS Sustain. Chem. Eng. 6 (10), 13378–13384.
Li, H., Zhang, W., Wang, J., Yang, Z., Li, L., Shih, K., 2018. Copper slag as a catalyst for mercury oxidation in coal combustion flue gas. Waste Manage. (Oxford) 74, 253–259.
Li, Y., Li, W., Liu, Q., Meng, H., Lu, Y., Li, C., 2018. Alkynyl carbon materials as novel and efficient sorbents for the adsorption of mercury(ii) from wastewater. J. Environ. Sci. 68, 169–176.
Liu, H., Xie, X., Chen, H., Yang, S., Liu, C., Liu, Z., et al., 2020. SO_2 promoted ultrafine nano-sulfur dispersion for efficient and stable removal of gaseous elemental mercury. Fuel 261, 116367.
Liu, Z., Li, Z., Xie, X., Yang, S., Fei, J., Li, Y., et al., 2020. Development of recyclable iron sulfide/selenide microparticles with high performance for elemental mercury capture from smelting flue gas over a wide temperature range. Environ. Sci. Technol. 54 (1), 604–612.
Liu, Z., Peng, B., Chai, L., Liu, H., Yang, S., Yang, B., et al., 2017. Selective removal of elemental mercury from high-concentration SO_2 flue gas by thiourea solution and investigation of mechanism. Ind. Eng. Chem. Res. 56 (15), 4281–4287.
Liu, Z., Wang, D., Peng, B., Chai, L., Liu, H., Yang, S., et al., 2017. Transport and transformation of mercury during wet flue gas cleaning process of nonferrous metal smelting. Environ. Sci. Pollut. Res. 24 (28), 22494–22502.
Liu, Z., Wang, D., Peng, B., Chai, L., Yang, S., Liu, C., et al., 2017. Mercury re-emission in the smelting flue gas cleaning process: the influence of arsenite. Energy Fuels 31 (10), 11053–11059.
Liu, Z., Wang, D., Yang, S., Liu, H., Liu, C., Xie, X., et al., 2019. Selective recovery of mercury from high mercury-containing smelting wastes using an iodide solution system. J. Hazard. Mater. 363, 179–186.
Liu, Z., Yang, S., Li, Z., Xie, X., Li, Y., Sun, Z., et al., 2019. Three-layer core-shell magnetic Fe_3O_4@C@Fe_2O_3 microparticles as a high-performance sorbent for the capture of gaseous arsenic from so2-containing flue gas. Chem. Eng. J. 378, 122075.
Ma, Y., Mu, B., Zhang, X., Zhang, H., Xu, H., Qu, Z., et al., 2019. Hierarchical Ag-SiO_2@Fe_3O_4 magnetic composites for elemental mercury removal from non-ferrous metal smelting flue gas. J. Environ. Sci. 79, 111–120.
Ma, Y., Xu, H., Qu, Z., Yan, N., Wang, W., 2014. Absorption characteristics of elemental mercury in mercury chloride solutions. J. Environ. Sci. 26 (11), 2257–2265.
Powell, A.C., Shibuta, Y., Guyer, J.E., Becker, C.A., 2007. Modeling electrochemistry in metallurgical processes. JOM 59 (5), 35–43.
Quijada, C., Huerta, F.J., Morallón, E., Vázquez, J.L., Berlouis, L.E.A., 2000. Electrochemical behaviour of aqueous SO_2 at polycrystalline gold electrodes in acidic media: a voltammetric and in situ vibrational study: Part 1. reduction of SO_2: deposition of monomeric and polymeric sulphur. Electrochim. Acta 45 (11), 1847–1862.
Robotin, B., Ispas, A., Coman, V., Bund, A., Ilea, P., 2013. Nickel recovery from electronic waste ii electrodeposition of Ni and Ni–Fe alloys from diluted sulfate solutions. Waste Manage. (Oxford) 33 (11), 2381–2389.
Tao, X., Li, K., Yan, H., Yang, H., Li, A., 2016. Simultaneous removal of acid green 25 and mercury ions from aqueous solutions using glutamine modified chitosan magnetic composite microspheres. Environ. Pollut. 209, 21–29.
Wang, Y., Xue, Y., Su, J., Zheng, S., Lei, H., Cai, W., et al., 2018. Efficient electrochemical recovery of dilute selenium by cyclone electrowinning. Hydrometallurgy 179, 232–237.
Wu, Q.R., Li, G.L., Wang, S.X., Liu, K.Y., Hao, J.M., 2018. Mitigation options of atmospheric Hg emissions in china. Environ. Sci. Technol. 52 (21), 12368–12375.
Xu, H., Li, B., Wei, Y., Wang, H., 2020. Extracting of copper from simulated leaching solution of copper-cadmium residues by cyclone electrowinning technology. Hydrometallurgy, 105298.
Yan, K., Liu, Z., Li, Z., Yue, R., Guo, F., Xu, Z., 2019. Selective separation of chromium from sulphuric acid leaching solutions of mixed electroplating sludge using phosphate precipitation. Hydrometallurgy 186, 42–49.
Yang, B., Chai, L., Zhu, F., Yan, X., Xiang, K., Liu, Z., et al., 2017. Selenium-assisted reduction of sulfur dioxide by carbon monoxide in the liquid phase. Ind. Eng. Chem. Res. 56 (8), 1895–1902.
Yang, J., Wang, Q., Zhou, J., Shen, Q., Cao, L., Yang, J., 2020. Electrochemical removal of gaseous elemental mercury in liquid phase with a novel foam titanium-based dsa anode. Sep. Purif. Technol. 250, 117162.
Yang, S., Liu, Z., Yan, X., Liu, C., Zhang, Z., Liu, H., et al., 2019. Catalytic oxidation of elemental mercury in coal-combustion flue gas over the cualo2 catalyst. Energy Fuels 33 (11), 11380–11388.
Yang, S., Wang, D., Liu, H., Liu, C., Xie, X., Xu, Z., et al., 2019. Highly stable activated carbon composite material to selectively capture gas-phase elemental mercury from smelting flue gas: Copper polysulfide modification. Chem. Eng. J. 358, 1235–1242.
Zhang, H., Wang, T., Zhang, Y., Sun, B., Pan, W.P., 2020. Promotional effect of Nh3 on mercury removal over biochar thorough chlorine functional group transformation. J. Clean. Prod. 257, 120598.
Zhang, L., Xu, Z., He, Z., 2020. Selective recovery of lead and zinc through controlling cathodic potential in a bioelectrochemically-assisted electrodeposition system. J. Hazard. Mater. 386, 121941.
Zhang, L., Yang, S., Lai, Y., Liu, H., Fan, Y., Liu, C., et al., 2020. In-situ synthesis of monodispersed cuxo heterostructure on porous carbon monolith for exceptional removal of gaseous Hg^0. Appl. Catal. B 265, 118556.
Zou, S., Liao, Y., Tan, W., Liang, X., Xiong, S., Huang, N., et al., 2017. H_2S-modified natural ilmenite: a recyclable magnetic sorbent for recovering gaseous elemental mercury from flue gas. Ind. Eng. Chem. Res. 56 (36), 10060–10068.